International Journal of Thermal Sciences 49 (2010) 797–808

Contents lists available at ScienceDirect

International Journal of Thermal Sciences

journal homepage: www.elsevier.com/locate/ijts

Buoyant heat transport in fluids across tilted square cavities discretely heated at one side

Massimo Corcione*, Emanuele Habib

Dipartimento di Fisica Tecnica, Sapienza University of Rome, via Eudossiana 18, 00184 Rome, Italy

ARTICLE INFO

Article history:
Received 12 March 2009
Received in revised form
18 November 2009
Accepted 25 November 2009
Available online 24 December 2009

Keywords:
Natural convection
Enclosure
Partial heating
Numerical analysis
Dimensionless correlations

ABSTRACT

Laminar natural convection heat transfer inside fluid-filled, tilted square cavities cooled at one side and partially heated at the opposite side, is studied numerically. A computational code based on the SIMPLE-C algorithm is used for the solution of the system of mass, momentum, and energy transfer equations. Simulations are performed for a complete range of heater sizes and locations, Rayleigh numbers based on the side of the cavity from 10^3 to 10^7, Prandtl numbers from 0.7 to 700, and tilting angles of the enclosure from -75° to $+75^\circ$, where negative angles correspond to configurations with the heater facing downwards. It is found that the heat transfer rate increases with increasing the Rayleigh and Prandtl numbers, and the size of the heater. In addition, for negative inclinations of the enclosure the amount of heat exchanged decreases with increasing the tilting angle, while for positive inclinations the heat transfer rate either increases or decreases according as the heater is located toward the top or the bottom of the cavity. Finally, as far as the heater location is specifically concerned, the heat transfer performance has a peak for intermediate positions, the higher are the Rayleigh and Prandtl numbers, as well as the tilting angle for positive inclinations, the closer to the bottom of the cavity is the optimum heater location for maximum heat removal.

1. Introduction

Natural convection heat transfer inside rectangular cavities with differentially heated sides and insulated top and bottom walls has been extensively studied, being of interest in numerous engineering applications, e.g., heat removal from electronic equipment, solar energy collection, and heat transfer in buildings. However, in many practical cases heating takes place just over a portion of one of the sidewalls, whose size and location may affect significantly the amount of heat transferred across the enclosure.

Natural convection inside air-filled, two-dimensional rectangular enclosures partially heated at one side and cooled at the opposite side was studied first by Chu et al. [1], who conducted a numerical parametric study for a complete range of heater sizes and locations, height-to-width aspect ratios of the cavity from 0.4 to 5, and Rayleigh numbers Ra_H based on the height of the cavity from 0 to 10^5. An experimental test of the accuracy of the solutions obtained was also executed for a square channel. It was found that the heat transfer rate across the enclosure increased with increasing either the heater size or the cavity aspect ratio, while showing a maximum at an optimum heater location, that shifted toward the bottom of the enclosure with increasing Ra_H. The numerical predictions of Chu et al. were then confirmed by Turner and Flack [2], who executed two-dimensional experiments by varying parametrically the height-to-width aspect ratio of the cavity H/W in the range between 0.5 and 2, the dimensionless heater size L/H in the range between 0.125 and 0.5, and the dimensionless heater location S/H in the range between 0.125 and 0.875, for $Pr = 0.7$ and Grashof numbers based on the cavity height of 5×10^6 to 9×10^6.

Keyhani et al. [3] conducted heat transfer experiments in an ethylene glycol-filled rectangular cavity of aspect ratio 16.5 with one isothermal vertical cold wall and eleven alternately unheated and flush-mounted rows of uniformly heated strips of equal height on the opposing vertical wall, for modified Rayleigh numbers based on the cavity width from 6×10^6 to 10^8. They found that the heat transfer coefficient generally decreased with increasing the elevation of the heater, although not uniformly, and that the average Nusselt number for the discrete heating case was substantially higher than that of a fully heated vertical cavity, which was ascribed to the inherent instability of the flow induced by the discrete heating.

Chadwick et al. [4] performed experiments and numerical simulations to study two-dimensional natural convection in an

* Corresponding author. Tel.: +39 06 44 58 54 43; fax: +39 06 48 80 120.
E-mail address: massimo.corcione@uniroma1.it (M. Corcione).

1290-0729/$ – see front matter © 2009 Elsevier Masson SAS. All rights reserved.
doi:10.1016/j.ijthermalsci.2009.11.012

air-filled rectangular cavity of aspect ratio $H/W = 5$ with single and multiple discrete heat sources mounted flush on one sidewall. The dimensionless heater length L/H for all the cases investigated was 0.133, while the modified Grashof number based on the heater length was varied between 10^4 and 10^7. For the single heat source configuration, dimensionless distances of the heater from the top of the enclosure $S/H = 0.2$, 0.5, and 0.8, were investigated. In contrast with the data of Chu et al. the average Nusselt number did not show any peak, rising monotonically with increasing S/H. However, it is worth pointing out that since Chadwick et al. based their modified Grashof number on the heater length rather than the cavity height, the buoyancy magnitude in their experiments and simulations was at least two orders higher than that imposed numerically by Chu et al. This, taking into account the relationship between the optimal heater location and the Rayleigh number observed by Chu et al. may possibly justify the results of Chadwick et al. For the dual heat source configuration, which was studied also for aspect ratios $H/W = 4$ and 6, heater locations of $S/H = 0.2$ and 0.5, and $S/H = 0.5$ and 0.8, were considered. As was the case of the single heater enclosure, a generally more effective cooling was detected when the discrete heating occurred toward the bottom of the cavity. In addition, it was found that the heat transfer from the lower heater was affected only marginally by the presence of the heater above, while the upper heater exhibited heat transfer degradations up to 40% owing to the influence of the thermal wake from the heat source below. Only minor effects on the heat transfer characteristics of the enclosure were observed with varying the cavity aspect ratio. Finally, in the multiple heat source configuration, the upper and lower heaters were at fixed locations $S/H = 0.2$ and 0.8, respectively, which left an unheated section of dimensionless length of 0.133 at the top and bottom of the enclosure. Three, four, or five heat sources were then equally spaced between the fixed adiabatic sections at the top and bottom. Moreover, the case of a continuously heated wall was also considered, for which the heater length was $L/H = 0.733$ with adiabatic sections at the cavity top and bottom having identical dimensionless length of 0.133. As expected, the heat sources located in the lower part of the cavity exhibited the highest heat transfer performance. In addition, in accordance with the results of Keyhani et al. it was found that the single continuous heater yielded generally lower local heat transfer coefficient than the multiple heat sources.

Refai Ahmed and Yovanovic [5,6] performed a twin numerical study on natural convection in air-filled square enclosures discretely heated at one side, with the opposite side entirely cooled. Results were obtained for Rayleigh numbers based on the heater length in the range between 0 and 10^6, and relative size of the heat source to the side of the enclosure in the range between 0.25 and 1, with the heater located either at the top or at the bottom of the discretely heated sidewall [5], or at the center of it [6]. It was found that when the heater was located either at the bottom or at the center of the sidewall, the average Nusselt number decreased with increasing the heater size, at least for Rayleigh numbers higher than nearly 300. This result is only apparently in disagreement with the results derived by Chu et al. and by Turner and Flack, who based their Rayleigh or Grashof numbers on the cavity height rather than the heater length. In fact, once the scale length is properly changed, the data of these authors show the same trend of those by Refai Ahmed and Yovanovic. In contrast, when the heat source was located at the top of the enclosure, the average Nusselt number was found to increase with the heater size, regardless of the Rayleigh number.

Ho and Chang [7] carried out a numerical investigation of natural convection in air-filled rectangular cavities with four isoflux heating strips mounted flush on one side, the other side being cooled at uniform temperature. The size of the heaters and their spacing, relative to the cavity height, were fixed at 1/30 and 13/75, respectively. Computations were performed for height-to-width aspect ratios of the enclosure in the range between 1 and 10, and modified Rayleigh numbers $(Ra_W)^*$ based on the cavity width in the range between 10^3 and 10^7. Experiments with a test cell of aspect ratio $H/W = 10$ were also executed to verify the accuracy of the numerical results. It was found that the average Nusselt number decreased with increasing the aspect ratio of the cavity, at a rate which decreased with $(Ra_W)^*$. Moreover, the thermal performance of the heaters decreased with their elevation, showing a difference which increased significantly with $(Ra_W)^*$.

Polentini et al. [8] reported experimental data for a 3×3 array of square heat sources mounted flush on one vertical wall of a liquid-filled rectangular cavity, whose opposite wall was cooled. The height-to-depth aspect ratio of the enclosure, as well the size and location of the nine heaters, were kept constant during the course of the investigation. In particular, the heater size and pitch, relative to the cavity height, were fixed at 0.133 and 0.166, respectively. Experiments were performed with FC-77 and water, for height-to-width aspect ratios of the cavity in the range between 2.5 and 7.5, Rayleigh numbers based on the heater side in the range between 10^5 and 10^8, and tilting angles of the cavity with respect to the gravity vector in the range between 0°, which corresponds to the vertical configuration, and 90°, which corresponds to the horizontal configuration with the heating elements located on the bottom of the enclosure. In the vertical configuration, besides heating all the nine elements, measurements were executed also by heating either individual rows of elements separately, in order to determine the effect of the heater location, or combinations of two rows of elements simultaneously, in order to determine the effect of both spacing and location of the heaters. When the heaters were powered simultaneously, the heat transfer performance resulted to be highest for the elements in the bottom row and lowest for the elements in the top row. As expected, the heat transfer performance of each row increased when the other rows were unheated, since the effect of the thermal plume was eliminated. Moreover, consistently with the data of previous researchers, the average Nusselt number of the individually heated rows was found to decrease with increasing the elevation of the row. Finally, the effects of the Prandtl number and the cavity aspect ratio were negligible, while the heat transfer performance of the heaters enhanced significantly with increasing the tilting angle of the test cell. Following the work of Polentini et al. several three-dimensional investigations of natural convection induced by the same 3×3 array of discrete heat sources were then performed by Heindel et al. [9,10], Tou et al. [11], Tou and Zhang [12], and Tso et al. [13], for different fluids and ranges of the modified Rayleigh number, the height-to-width aspect ratio of the enclosure, and the tilting angle of the enclosure.

Liu and Phan-Tien [14] investigated numerically the optimum spacing problem for three elements generating heat at uniform rate per unit volume, mounted on a vertical conductive substrate inside an air-filled rectangular enclosure cooled at the opposite sidewall. The rear of the conducting substrate, as well as the top and bottom walls of the enclosure, were assumed adiabatic. The height-to-width aspect ratio of the enclosure, and the thickness of the conductive substrate relative to the cavity width, were fixed at 7/4 and 1/16, respectively. The ratio between the heights of the heater and the cavity, and the ratio between the widths of the heater and the cavity, were fixed at 1/7 and 1/8, respectively. Simulations were conducted for Rayleigh numbers based on the heat generation rate of 10^4 and 10^5, and 14 different arrangements of the heating elements. A thermal performance better than that typical of the conventional equispaced setting was obtained when the center-to-center distance among the heaters from bottom to top followed

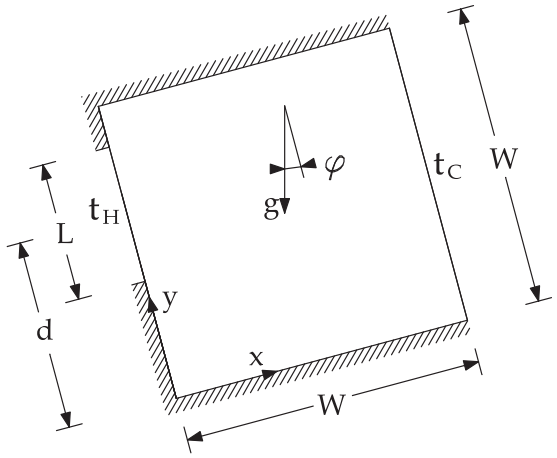

Fig. 1. Sketch of the geometry and coordinate system.

a geometric series, especially when the geometric ratio was the golden mean, i.e., 1.618, which implied improvements of the order of 10%.

The optimal distribution of discrete heat sources mounted on the inside of one of the sidewalls of an air-filled square enclosure cooled at the opposite wall was studied numerically some years later by da Silva et al. [15,16] under the assumption of isoflux heaters, for modified Rayleigh numbers in the range between 10^2 and 10^6, and heights of the heaters relative to the cavity size in the range between 0.05 and 0.2. Computations were executed for a single heater, and for two and three heat sources. For the single heater, it was shown that the optimal location for maximum heat transfer migrated toward the bottom of the cavity with increasing the Rayleigh number. The same qualitative trend was observed for the multiple heat sources, which was in accordance with the results of Liu and Phan-Tien.

Frederick and Quiroz [17] performed a numerical study on air-filled cubical enclosures with a cold vertical wall and a hot square sector located in the center of the opposite wall, for Rayleigh numbers based on the cavity side in the range between 10^3 and 10^7, and values of the ratio between the side of the heater and the side of the cavity in the range between 0.3 and 0.7. For any size of the heater, a dimensionless correlation between the average Nusselt number and the Rayleigh number in the range between 10^5 and 10^7 was derived. Two-dimensional results for a square cavity with a heater of dimensionless size of 0.5 were also obtained at different Rayleigh numbers.

He et al. [18] carried out a numerical parametric analysis on liquid-filled parallelepipedal enclosures with a square vertical wall of side H cooled at uniform temperature and two square isothermal heaters of side L located one above the other at the center of the opposite square vertical wall. Two relative sizes of the heaters $L/H = 0.2$ and 0.3 were considered, while the dimensionless distance between them was fixed at 0.1. Computations were executed for different values of the height-to-width aspect ratio of the cavity in the range between 0.625 and 20, Rayleigh numbers Ra_H based on the cavity height in the range between 10^3 and 10^7, and Prandtl numbers in the range between 5 and 140. It was found that the effect of the Prandtl number was practically negligible. Furthermore, an optimal height-to-width aspect ratio of the cavity for maximum heat transfer from both sources of approximately 5–10 was detected at $Ra_H = 10^6$–10^7. Finally, the heat transfer rate at the top heater resulted always lower than that at the bottom heater, regardless of the Rayleigh number and the cavity aspect ratio.

Quite recently, Baïri et al. [19] performed an experimental and numerical study on vertical and inclined air-filled cubic enclosures with one sidewall cooled at uniform temperature, and the opposite wall consisting of five superimposed strips of same height, alternately heated at uniform temperature and adiabatic. Results and correlations were reported for Rayleigh numbers based on the strip height in the range between 10^3 and 3×10^8, and tilting angles with respect to gravity in the range between $-90°$ and $+90°$, showing a substantial good agreement with prior literature data.

Other works with a bearing on the subject discussed here are those wherein also the cooled wall is only partially active, which is for example the case of the studies brought forth by Nithyadevi et al. [20] and Deng [21].

The above review of the existing literature shows that the main phenomenologic aspects of the problem are well understood, but, at same time, the data available lack to a large extent of generality. In fact, as most studies either deal with too specific configurations, see refs. [3,4,7–14,17,19–21], or are characterized by a parametric approach, see refs. [1,2,18], the use of the results obtained for design purposes is extremely limited. In this perspective, it seems that the only data with fairly wide ranges of applicability are those derived by Refai Ahmed and Yovanovic [5,6], although these authors did not take into full account the effects of the position of the heat source, and consequently did not determine the optimal heater location for maximum heat transfer observed by other authors. From this viewpoint, useful results are those obtained by da Silva et al. [15,16], although they considered only heaters with a rather limited size. In addition, the aforementioned works by Refai Ahmed and Yovanovic, and by da Silva et al. do not take into account either the effects of the working fluid or the effects of the inclination of the cavity with respect to gravity.

Table 1
Grid sensitivity analysis at $Ra = 10^4$ and $\varphi = 0°$, and $Ra = 10^6$ and $\varphi = 0°$ and 60°.

Ra	φ	$\Delta\tau$	Mesh size	Nu_H	%	Nu_C	%	U_{max}	%	V_{max}	%	Exec time
10^4	0°	10^{-3}	20 × 20	3.834	*−0.55*	1.919	*−0.45*	2.081	*−2.29*	2.348	*−3.50*	1′44″
			40 × 40	3.855	*−0.07*	1.928	*−0.09*	2.130	*−0.24*	2.433	*−0.98*	2′31″
			52 × 52	3.858	*−0.05*	1.929	*−0.06*	2.136	*−0.15*	2.457	*−0.50*	3′29″
			60 × 60	3.860	*0.00*	1.930	*0.00*	2.139	*0.00*	2.469	*0.00*	4′08″
10^6	0°	10^{-4}	40 × 40	14.714	*5.36*	7.358	*5.38*	17.933	*−2.47*	24.104	*−10.38*	7′26″
			60 × 60	13.965	*0.93*	6.982	*0.86*	18.386	*−0.18*	26.895	*−1.01*	13′26″
			80 × 80	13.837	*0.35*	6.923	*0.49*	18.419	*0.02*	27.168	*−0.29*	22′27″
			100 × 100	13.789	*0.00*	6.888	*0.00*	18.415	*0.00*	27.248	*0.00*	38′02″
10^6	60°	10^{-4}	40 × 40	13.770	*4.07*	6.883	*4.09*	42.511	*−2.48*	33.050	*−1.37*	8′38″
			60 × 60	13.231	*0.85*	6.612	*0.76*	43.592	*−0.46*	33.507	*−0.95*	15′36″
			80 × 80	13.120	*0.08*	6.562	*0.23*	43.794	*−0.44*	33.827	*−0.04*	24′00″
			100 × 100	13.109	*0.00*	6.547	*0.00*	43.987	*0.00*	33.840	*0.00*	41′01″

Table 2
Time-step sensitivity analysis at Ra = 10^6 and $\varphi = 0°$.

Ra	φ	Mesh size	$\Delta\tau$	Nu_H	%	Nu_C	%	U_{max}	%	V_{max}	%	Exec time
10^6	0°	80 × 80	10^{-2}	15.107	*3.00*	7.663	*2.50*	19.180	*1.10*	28.098	*2.40*	5′46″
			10^{-3}	14.667	*6.00*	7.476	*8.00*	18.972	*3.00*	27.440	*1.00*	6′50″
			10^{-4}	13.837	*0.01*	6.923	*0.01*	18.419	*0.01*	27.168	*0.01*	22′27″
			10^{-5}	13.836	*0.00*	6.922	*0.00*	18.418	*0.00*	27.166	*0.00*	1h50′45″

In this framework, the aim of the present paper is to carry out a numerical investigation of natural convection heat transfer inside tilted square cavities with one side cooled at uniform temperature, and the opposite side partially heated by an isothermal source, in order to derive heat transfer correlations spanning across ranges of the independent variables sufficiently wide to be of help in thermal engineering applications. The study is performed under the assumption of two-dimensional laminar flow, for a complete range of heater sizes and locations, Rayleigh numbers based on the side of the cavity from 10^3 to 10^7, Prandtl numbers from 0.7 to 700, and tilting angles of the enclosure from −75° to +75°. The horizontal and sub-horizontal configurations, which correspond to tilting angles around ±90°, are out of the scopes of the present investigation. In fact, at such inclinations the flow patterns differ significantly from the basic single cell that forms when the tilting angle of the enclosure is varied between −75° and +75°. In particular, when the enclosure is set horizontally with the heater facing upwards, complex flows related to Rayleigh-Bénard convection typically occur, which may give rise to unsteady solutions, as reported in the literature for both shallow and slender cavities – see, e.g., Yang [22], and Cappelli D'Orazio et al. [23]. In this perspective, the fundamental heat transfer features of horizontal and sub-horizontal configurations are deemed to deserve a specific study.

Regarding the primary technical interests of this investigation, it is worth pointing out that the configuration analysed here is strictly related with one of the fundamental problems in the cooling of electronic devices, that is, the optimal positioning of a discrete heat source in a fixed volume with natural convection. In fact, in many situations heat transfer designers prefer to avoid the use of mechanical fans or other active equipment for the fluid circulation, due to power consumption, excessive operating noise, or reliability concerns. On the other hand, in modern electronic assemblies a large number of high power dissipating components are often packaged in modular enclosures such that space and external cooling sources are minimal. Hence, the placement of these components within their enclosure requires to be optimized as to maximize the heat removal, which is the basic commitment of the present study.

2. Mathematical formulation

A fluid-filled, square enclosure of width W is cooled at one side, and partially heated at the opposite side. The discrete heat source, of length L, whose center is located at a distance d from the bottom wall of the enclosure, is kept at uniform temperature t_H, while the cooled side is maintained at temperature t_C. The remaining upper and lower parts of the heated sidewall, as well as the top and bottom walls of the cavity, are considered perfectly insulated. A zero surface emissivity is assumed for the confining walls, which physically corresponds to perfectly polished surfaces, thus implying that the present situation involves pure natural convection, i.e., absence of surface-to-surface radiation. The enclosure is tilted at an angle φ with respect to the gravity vector, as depicted in Fig. 1, in which the (x,y) coordinate system adopted and the thermal state of the boundary walls are also represented.

The flow is assumed to be two-dimensional, laminar and incompressible, with constant fluid properties and negligible viscous dissipation and pressure work. The buoyancy effects on momentum transfer are taken into account through the customary Boussinesq approximation.

Once the above assumptions are employed in the conservation equations of mass, momentum and energy, the following set of governing equations is obtained:

$$\nabla\cdot\mathbf{V} = 0 \tag{1}$$

$$\frac{\partial V}{\partial\tau} + (V\cdot\nabla)\mathbf{V} = -\nabla P + \nabla^2\mathbf{V} - \frac{\mathrm{Ra}}{\mathrm{Pr}}T\frac{\mathbf{g}}{g} \tag{2}$$

$$\frac{\partial T}{\partial\tau} + (\mathbf{V}\cdot\nabla)T = \frac{1}{\mathrm{Pr}}\nabla^2 T \tag{3}$$

where $\mathbf{V}$ is the velocity vector having dimensionless velocity components U and V normalized by ν/W, T is the dimensionless temperature excess over the uniform temperature of the cooled sidewall normalized by the temperature difference $(t_H - t_C)$, τ is the dimensionless time normalized by W^2/ν, P is the dimensionless pressure normalized by $\rho\nu^2/W^2$, $\mathbf{g}$ is the gravity vector, $\mathrm{Pr} = \nu/\alpha$ is the Prandtl number, and Ra is the Rayleigh number defined as:

$$\mathrm{Ra} = \frac{g\beta(t_H - t_C)W^3}{\alpha\nu} \tag{4}$$

Table 3
Comparison of the present solutions with the benchmark solutions of de Vahl Davis (BM1), Mahdi and Kinney + Hortman et al. (BM2), Wan et al. by FEM (BM3), and Wan et al. by DSC (BM4) for a differentially heated square cavity at steady-state.

Quantities	Present work	BM1	BM2	BM3	BM4
Ra = 10^3					
U_{max}	3.654	3.649	3.649	3.489	3.643
V_{max}	3.708	3.697	3.690	3.686	3.686
Nu	1.116	1.118	1.113	1.117	1.073
Ra = 10^4					
U_{max}	16.242	16.178	16.180	16.122	15.967
V_{max}	19.714	19.617	19.629	19.790	19.980
Nu	2.254	2.243	2.244	2.254	2.155
Ra = 10^5					
U_{max}	35.008	34.730	34.739	33.390	33.510
V_{max}	68.109	68.590	68.639	70.630	70.810
Nu	4.506	4.519	4.521	4.598	4.352
Ra = 10^6					
U_{max}	65.226	64.630	64.836	65.400	65.550
V_{max}	221.598	219.360	220.461	227.110	227.240
Nu	8.879	8.800	8.825	8.976	8.632

BM1 = de Vahl Davis [28].
BM2 = Mahdi and Kinney [29], for Ra = 10^3, and Hortman et al. [30], for Ra = 10^4–10^6.
BM3 = Wan et al. – FEM [31].
BM4 = Wan et al. – DSC [31].

Table 4
Comparison of the present solutions with the solutions of Frederick and Quiroz for an air-filled, untilted square cavity with $E = 0.5$ and $D = 0.5$ at steady-state.

Ra	$E = 0.5$, $D = 0.5$, $\varphi = 0°$, Pr = 0.7	Nu_H
10^3	Present work	0.985
	Frederick and Quiroz [17]	1.000
10^4	Present work	1.879
	Frederick and Quiroz [17]	1.831
10^5	Present work	3.630
	Frederick and Quiroz [17]	3.455
10^6	Present work	6.737
	Frederick and Quiroz [17]	6.788

Other parameters which enter into this study are:

(a) the dimensionless size of the heater

$$E = \frac{L}{W} \quad 0.1 \le E \le 1 \tag{5}$$

(b) the dimensionless location of the heater

$$D = \frac{d}{W} \quad E/2 \le D \le 1 - E/2 \tag{6}$$

The boundary conditions assumed are: (a) $T = 1$ and $\mathbf{V} = 0$ at the heated surface; (b) $T = 0$ and $\mathbf{V} = 0$ at the cooled surface; and (c) $\partial T/\partial n = 0$ and $\mathbf{V} = 0$ at the adiabatic surfaces, where n denotes the normal to the surface.

The initial conditions assumed are fluid at rest, i.e., $\mathbf{V} = 0$, and uniform temperature $T = 0$ throughout the whole cavity.

3. Computational procedure

The set of governing eqs. (1)–(3) along with the boundary and initial conditions stated above is solved through a control-volume formulation of the finite-difference method. The pressure-velocity coupling is handled through the SIMPLE-C algorithm described by Van Doormaal and Raithby [24], which is essentially a more implicit variant of the SIMPLE algorithm developed by Patankar and Spalding [25]. The QUICK discretization scheme proposed by Leonard [26] is used for the evaluation of the interface fluxes. A second-order backward scheme is used for time stepping. Starting from the assigned initial fields of the dependent variables across the cavity, at each time-step the discretized governing equations are solved iteratively through a line-by-line application of the Thomas algorithm, enforcing under-relaxation to ensure convergence. Details on the SIMPLE procedure, as well as on enhanced variants of the basic algorithm, may be found in Patankar [27].

Table 5
Comparison of the present results for the optimum heater location with the data obtained by da Silva et al. for an air-filled, untilted square cavity with $E = 0.2$ at steady-state.

Ra	$E = 0.2$, $\varphi = 0°$, Pr = 0.7	D_{opt}
10^3	Present work	0.490
	da Silva et al. [15]	0.483
10^4	Present work	0.440
	da Silva et al. [15]	0.433
10^5	Present work	0.380
	da Silva et al. [15]	0.371
10^6	Present work	0.300
	da Silva et al. [15]	0.292

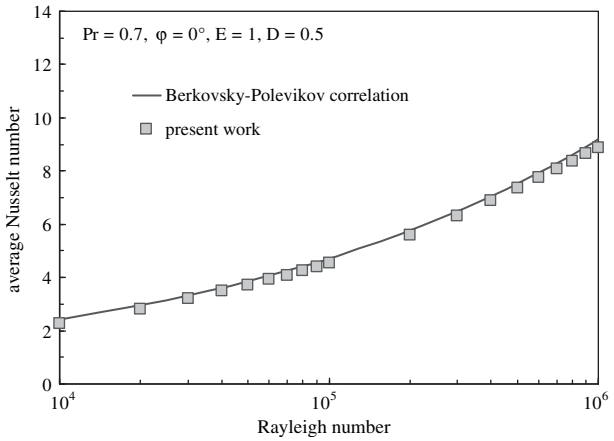

Fig. 2. Comparison between the present numerical results and the Berkovsky–Polevikov correlation for an air-filled, upright enclosure heated over the entire sidewall.

The computational spatial domain is covered with a non-uniform grid, having a higher concentration of grid lines near the boundary walls and both ends of the heat source, and a uniform spacing throughout the remainder interior of the cavity. Time discretization is chosen uniform. Within each time-step, the spatial solution is considered to be converged when the maximum absolute values of both the mass source and the relative changes of the dependent variables at any grid-node from iteration to iteration are smaller than the prescribed values, i.e., 10^{-4} and 10^{-5}, respectively. Time-integration is stopped once steady-state is reached. This means that the simulation procedure ends when the relative difference between the incoming and outgoing heat transfer rates, and the relative changes of the time-derivatives of the dependent variables at any grid-node between two consecutive time-steps, are smaller than the pre-set values, i.e., 10^{-6} and 10^{-7}, respectively.

Once steady-state is reached, the average Nusselt numbers Nu_H and Nu_C of the heater and the cooled wall, respectively, are calculated:

$$Nu_H = \frac{q_{in} W}{kL(t_H - t_C)} = \frac{Q_{in} W}{L} = \frac{1}{E} Q_{in} = -\frac{1}{E} \int_{D-E/2}^{D+E/2} \frac{\partial T}{\partial X}\bigg|_{X=0} dY \tag{7}$$

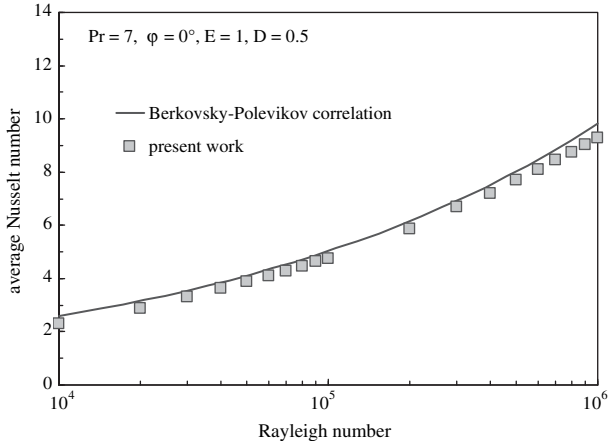

Fig. 3. Comparison between the present numerical results and the Berkovsky–Polevikov correlation for a water-filled, upright enclosure heated over the entire sidewall.

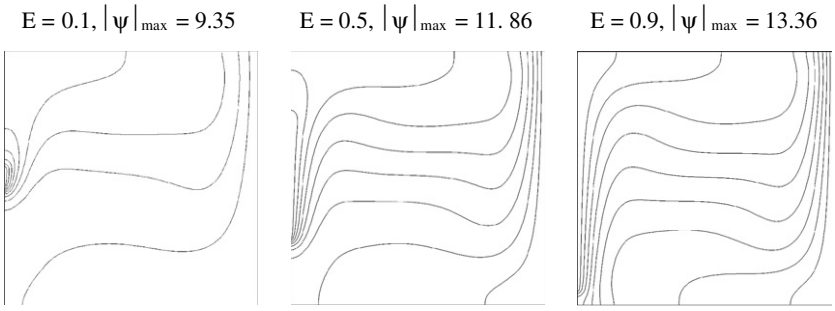

Fig. 4. Isotherm contours for $D = 0.5$, $\mathrm{Ra} = 10^5$, $\varphi = 0^\circ$, $\mathrm{Pr} = 0.7$ and $E = 0.1 - 0.9$.

$$\mathrm{Nu_C} = \frac{q_{\mathrm{out}} W}{\mathrm{kW}(t_\mathrm{C} - t_\mathrm{H})} = Q_{\mathrm{out}} = -\int_0^1 \left.\frac{\partial T}{\partial X}\right|_{X=1} dY \tag{8}$$

where q_{in} and q_{out} are the heat transfer rates per unit length added to the fluid by the heater and withdrawn from the fluid by the cooled sidewall, respectively, and $Q_{\mathrm{in}} = q_{\mathrm{in}}/k(t_\mathrm{H} - t_\mathrm{C})$ and $Q_{\mathrm{out}} = -q_{\mathrm{out}}/k(t_\mathrm{H} - t_\mathrm{C})$ are the corresponding dimensionless variables. The temperature gradients are evaluated by a second-order profile accounting for the wall-node and the two adjacent fluid-nodes.

Of course, since at steady-state the incoming and outgoing heat transfer rates per unit length are the same, that is, $q_{\mathrm{in}} = -q_{\mathrm{out}} = q$, and then $Q_{\mathrm{in}} = -Q_{\mathrm{out}} = Q$, the following relationship between $\mathrm{Nu_H}$ and $\mathrm{Nu_C}$ holds:

$$\mathrm{Nu_H} = \frac{\mathrm{Nu_C}}{E} \tag{9}$$

Tests on the dependence of the results on both grid size and time-step have been performed for several combinations of the parameters E, D, φ, Ra, and Pr. The optimal grid size and time-step used for computations are such that further refinements do not yield for noticeable modifications either in the heat transfer rates or in the flow field, that is, the percentage changes of $\mathrm{Nu_H}$ and $\mathrm{Nu_C}$, and those of the maximum velocity components $U_{\max}$ and $V_{\max}$ on the Y-wise and X-wise midplanes of the enclosure, are smaller than a prescribed accuracy value, i.e., 1%. In addition, the percentage difference between the first and second members of eq. (9) has to be smaller than 0.5%. Typically, the number of nodal points and time stepping used for computations lie in the ranges between 40×40 and 120×120, and between 10^{-6} and 10^{-3}, respectively. Selected results of the grid sensitivity analysis are presented for $E = 0.5$, $D = 0.5$, and $\mathrm{Pr} = 0.7$, in Table 1, in which the values of $\mathrm{Nu_H}$, $\mathrm{Nu_C}$, $U_{\max}$, and $V_{\max}$, and their respective percent changes between consecutive grid configurations, are reported. For any grid size, the execution times needed to reach the steady-state are also indicated. It may be seen that a denser grid is required at higher Rayleigh numbers – note that a grid size of 52×52 is deemed to be adequate at $\mathrm{Ra} = 10^4$ and $\varphi = 0^\circ$, while a grid size of 80×80 is necessitated at $\mathrm{Ra} = 10^6$ and $\varphi = 0^\circ$. In contrast, the grid-spacing is practically insensitive to the cavity inclination – note that at $\mathrm{Ra} = 10^6$ the same grid size of 80×80 gives acceptable results for both $\varphi = 0^\circ$ and $\varphi = 60^\circ$. As regards the time stepping, its effects are shown in Table 2 for $\mathrm{Ra} = 10^6$, $\varphi = 0^\circ$, $E = 0.5$, $D = 0.5$, and $\mathrm{Pr} = 0.7$. It may be observed that the quality of the asymptotic solution of the integration procedure depends very few on the time-step, provided that the time-step is sufficiently short. In this perspective, the time-steps used for computations were as long as possible in order to reach a compromise between solution accuracy and computation time. Note that the execution times reported in Tables 1 and 2 pertain to simulations performed by a personal computer equipped with a Quad-Core 9650 processor. From their analysis, it is evident that, for the assigned precision, the computation time depends mainly on the Rayleigh number, and much less on the cavity inclination.

Moreover, some test runs have also been executed with the initial uniform dimensionless temperature of the fluid set to 0.5 or 1, with the scope to determine what effect these initial conditions could have on the steady-state flow and temperature patterns. Asymptotic solutions practically identical to those obtained assuming $T = 0$ throughout the enclosure at $\tau = 0$ were obtained for all the configurations examined.

Finally, in order to validate the numerical code used for the present study, the steady-state solutions obtained for $\tau \to \infty$ in a vertical square cavity with differentially heated sides and adiabatic top and bottom walls for Rayleigh numbers from 10^3 to 10^6, have been compared with the benchmark results obtained by de Vahl Davis [28] through a standard finite-difference method, as shown in Table 3. In particular, the average Nusselt numbers as well as the maximum horizontal and vertical velocity components, on the vertical and horizontal midplanes, respectively, are well within 1% of the benchmark data listed in column BM1. The following

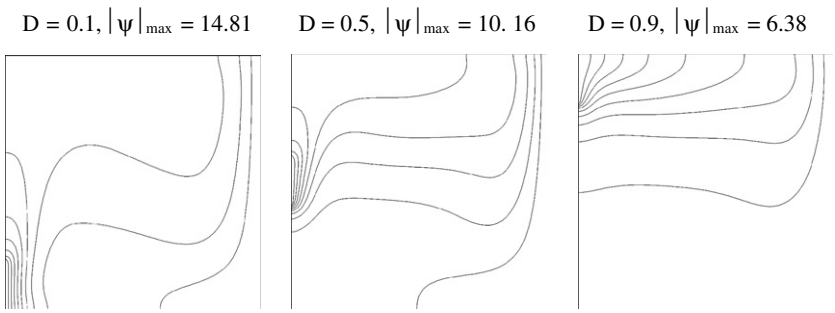

Fig. 5. Isotherm contours for $E = 0.2$, $\mathrm{Ra} = 10^5$, $\varphi = 0^\circ$, $\mathrm{Pr} = 0.7$ and $D = 0.1 - 0.9$.

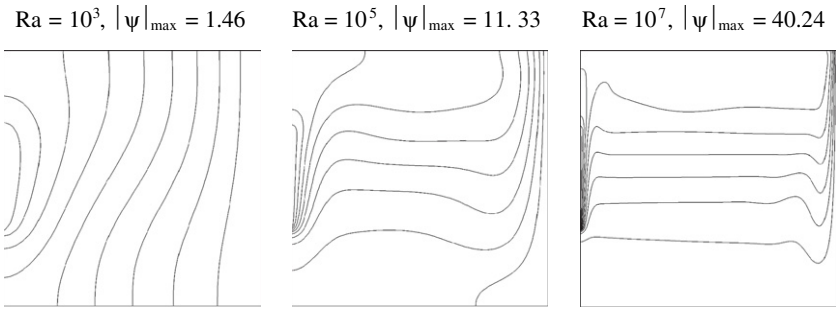

Fig. 6. Isotherm contours for $E = 0.4$, $D = 0.5$, $\varphi = 0^\circ$, Pr = 0.7 and Ra = 10^3–10^7.

additional benchmark solutions are also reported for further comparison: (a) the results obtained through finite-volume methods by Mahdi and Kinney [29], for Ra = 10^3, and by Hortman et al. [30], for Ra = 10^4 to 10^6, are listed in column BM2; (b) the results obtained through a finite-element method by Wan et al. [31] are listed in column BM3; and (c) the results obtained through a discrete singular convolution algorithm by Wan et al. [31] are listed in column BM4. It is worth noticing that our dimensionless velocity results have been multiplied by the Prandtl number before being inserted in Table 3, so as to account for the choice of the ratio between kinematic viscosity of the fluid and characteristic length as scale factor for the velocity, instead of the ratio between thermal diffusivity of the fluid and characteristic length, used in refs. [28] to [31]. In addition, the average Nusselt numbers Nu_H obtained from the simulations performed for $\varphi = 0^\circ$ and Pr = 0.7 are compared with the two-dimensional data of Frederick and Quiroz [17] for $E = 0.5$, $D = 0.5$, and Ra = 10^3 to 10^6, as reported in Table 4, where an overall good degree of agreement may be observed, with a maximum percentage difference of 5%. Moreover, the optimum heater location for maximum heat transfer D_{opt} derived through the simulations carried out for $E = 0.2$, $\varphi = 0^\circ$ and Pr = 0.7 are compared with the data of da Silva et al. [15] for Ra = 10^3 to 10^6, as reported in Table 5. Also in this case, the concordance between the present results and the literature data is rather good, with a maximum percentage difference lower than 3%. The validation of the simulation procedure terminates with a comparison between the average Nusselt numbers $Nu_H \equiv Nu_C$ computed numerically for $\varphi = 0^\circ$, $E = 1$, $D = 0.5$, and Ra = 10^4 to 10^6, and the usually recommended Berkovsky–Polevikov correlation based on experimental and numerical data of laminar natural convection in a rectangular cavity heated and cooled from the side with an aspect ratio near unity [32,33]. For both cases of Pr = 0.7 and Pr = 7, displayed in Figs. 2 and 3, respectively, the correspondence between numerical and literature data is widely satisfactory.

4. Results and discussion

Numerical simulations are performed for different values of (a) the dimensionless size of the heater, E, in the range between 0.1 and 1, (b) the dimensionless location of the heater, D, in the range between $E/2$ and $(1 - E/2)$, (c) the tilting angle of the enclosure with respect to the gravity vector, φ, in the range between -75° and $+75^\circ$, where negative or positive angles correspond to configurations with the heater facing either downwards or upwards, (d) the Rayleigh number based on the side of the enclosure, Ra, in the range between 10^3 and 10^7, and (e) the Prandtl number, Pr, in the range between 0.7 and 700.

The discussion of the results is organized as follows: the data for Pr = 0.7, which corresponds to air, are reported and discussed first, in order to stress the effects of the heater size and location, the Rayleigh number, and the tilting angle, on the thermal performance of the enclosure; subsequently, emphasis is given to the effects of the Prandtl number; finally, a set of dimensionless correlating equations is proposed.

A selection of local results for Pr = 0.7 is presented in Figs. 4–9, where isotherm contours, corresponding to equispaced values of the dimensionless temperature T in the range between 0 and 1, are plotted for different sets of values of E, D, Ra, and φ, in order to highlight the effects of these independent variables on the temperature field, and then on the amount of heat exchanged at the heater surface. As regards the fluid motion, the related streamline plots are omitted for the sake of brevity. Indeed, as expected, for all the configurations examined the flow field consists basically of a single roll-cell that derives from the rising of the hot fluid adjacent to the heater and its descent along the opposite cooled sidewall. For each configuration examined, indications on the rate of fluid circulation are given in terms of $|\psi|_{max}$, i.e., the maximum absolute value of the dimensionless stream function ψ, that is defined as usual through $U = \partial\Psi/\partial Y$ and $V = -\partial\Psi/\partial X$.

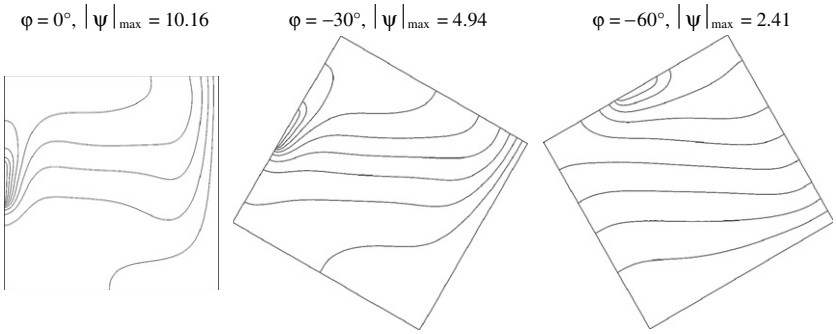

Fig. 7. Isotherm contours for $E = 0.2$, $D = 0.5$, Ra = 10^5, Pr = 0.7 and $\varphi = 0^\circ$ to -60°.

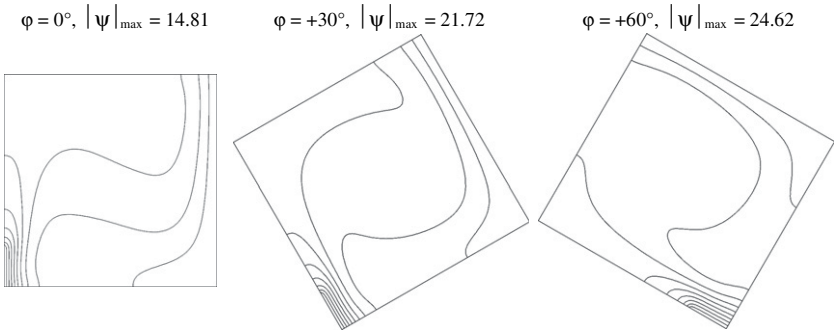

Fig. 8. Isotherm contours for $E = 0.2$, $D = 0.1$, $\mathrm{Ra} = 10^5$, $\mathrm{Pr} = 0.7$ and $\varphi = 0°$ to $+60°$.

As far as the overall results are concerned, the heat transfer performance of the cavity is expressed in terms of the average Nusselt number of the cooled sidewall $\mathrm{Nu_C}$, which is considered more suitable for this purpose than that of the heater $\mathrm{Nu_H}$. In fact, once both Ra and D are assigned, the amount Q of heat transferred across the cavity obviously increases as the length E of the heater increases, regardless of the tilting angle and the Prandtl number. Correspondingly, a Nusselt number which would describe the thermal behavior of the cavity "at a glance" should increase with increasing E. Actually, according to eq. (7), $\mathrm{Nu_H} = Q/E$, thus implying that $\mathrm{Nu_H}$ may either increase or decrease with increasing E, depending on whether $\partial Q/\partial E$ is positive or negative. In contrast, based on eq. (8), $\mathrm{Nu_C} = Q$, which means that $\mathrm{Nu_C}$ unequivocally increases with E. On the other hand, the Nusselt number $\mathrm{Nu_C}$ coincides with the average Nusselt number of the heater Nu^* when the heater size L is used as characteristic length instead of the width W of the cavity:

$$\mathrm{Nu}^* = \frac{q_{\mathrm{in}} L}{\mathrm{kL}(t_{\mathrm{H}} - t_{\mathrm{C}})} = Q_{\mathrm{in}} = E \cdot \mathrm{Nu_H} = \mathrm{Nu_C} \tag{10}$$

Indeed, as Nu^* represents the dimensionless amount of thermal power exchanged at the heater surface, it delivers a straight information on the effectiveness of heat removal from the discrete source rather than $\mathrm{Nu_H}$, which is nothing more than the dimensionless counterpart of the average coefficient of convection of the heater. Typical distributions of the average Nusselt number Nu^* for $\mathrm{Pr} = 0.7$ are reported in Figs. 10–12. In particular: (a) Fig. 10 illustrates the dependence of Nu^* on Ra for $\varphi = 0°$, with E and D as parameters; (b) Fig. 11 illustrates the dependence of Nu^* on D for $\varphi = 0°$ and $E = 0.2$, with Ra as a parameter; and (c) Fig. 12 illustrates the dependence of Nu^* on φ for $E = 0.2$ and $\mathrm{Ra} = 10^5$, with D as a parameter.

It is worth noticing that the size and location of the heater have a direct influence upon the motion intensity. In fact, since the fluid below the heater tends to remain relatively stagnant (see Figs. 4 and 5), the enclosure is more significantly affected by the buoyancy-driven flow when the discrete source is either larger or occupies a position lower in the cavity, as clearly denoted by the higher values of $|\psi|_{\max}$ with increasing E and decreasing D. Thus, at any given value of D, the effectiveness of the heat source cooling enhances with increasing the heater size E (see Fig. 10, empty-symbol distributions for $D = 0.5$). In contrast, once E is fixed, the heat transfer performance of the enclosure does not vary monotonically with D (see Fig. 10, full-symbol distributions for $E = 0.2$), showing a peak for a location of the heater that moves toward the bottom of the cavity as the Rayleigh number increases (see Fig. 11), which is in full accordance with what was previously predicted by Chu et al. and later confirmed experimentally by Turner and Flack and numerically by da Silva et al. The existence of an optimum heater position for maximum heat removal may be explained by considering that, in this case, what counts is not only the motion intensity, but also the shape of the recirculation cell. In fact, when the discrete source is located too close to either the bottom or the top wall of the enclosure, the rising jet of fluid cannot wash the entire surface of the heater, thus implying that the amount of heat exchanged by its lower or upper portion, respectively, is smaller than that correspondingly exchanged when the heater is located at mid-height. This is, e.g., shown in Fig. 13, where the distributions of the local Nusselt number along the surface of the discrete source $[-(\partial T/\partial X)]_{X=0}$ are plotted for $\varphi = 0°$, $\mathrm{Ra} = 10^5$, $E = 0.2$, and three different values of D. However, as expected, the influence of the heater location on the heat transfer rate has resulted to decrease with increasing E, up to vanishing for $E > 0.6$.

As far as the effects of the Rayleigh number are concerned (see Fig. 6), it may be seen that at $\mathrm{Ra} = 10^3$ the isotherm lines are nearly vertical in most of the enclosure, denoting the conduction-

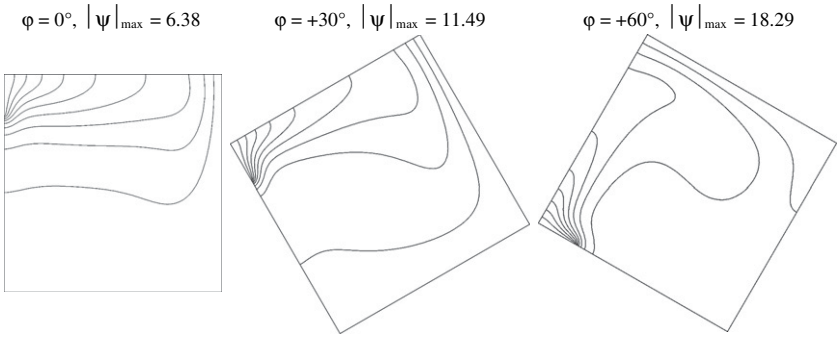

Fig. 9. Isotherm contours for $E = 0.2$, $D = 0.9$, $\mathrm{Ra} = 10^5$, $\mathrm{Pr} = 0.7$ and $\varphi = 0°$ to $+60°$.

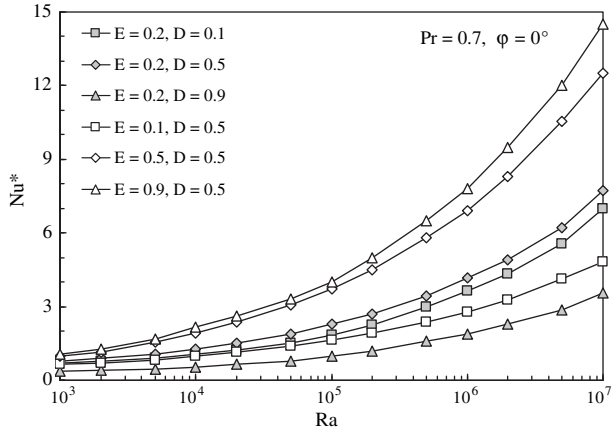

Fig. 10. Distributions of Nu* vs. Ra for Pr = 0.7, $\varphi = 0°$, and six combinations of E and D.

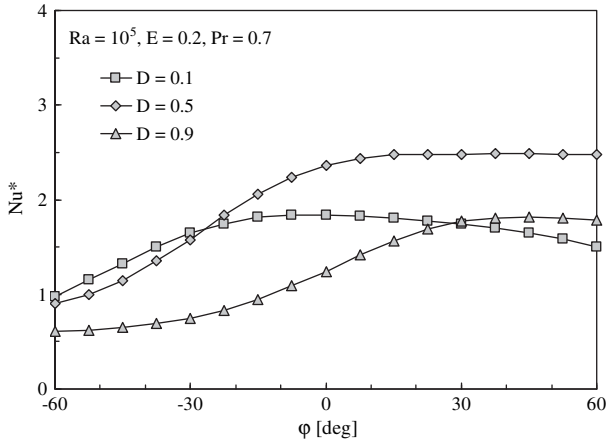

Fig. 12. Distributions of Nu* vs. φ for Pr = 0.7, $E = 0.2$, Ra = 10^5 and $D = 0.1-0.9$.

dominated heat transfer mechanism. As Ra gets higher, and then the buoyancy forces increases more and moreover the viscous forces, the isotherm lines are progressively more distorted and warped around the center of rotation, and at same time compressed toward the thermally active walls, which leads to an enhancement of the heat transfer rate (see Figs. 10 and 11). At Ra = 10^6 the formation of thin boundary layers adjacent to the heater and the cooled wall, and the contemporary well defined horizontal fluid stratification in the middle of the cavity, reflect that advection is the dominant heat transfer mechanism inside the enclosure.

The effects of the tilting angle of the cavity differ according as the inclination is positive or negative, i.e., depending on the fact that the heater faces upwards or downwards, and according as D is small or large. For negative tilting angles (see Fig. 7), the motion intensity decreases significantly and the fluid tends to get increasingly more stratified as the inclination of the cavity increases, which degrades the heat transfer performance of the enclosure, regardless of the heater position (see Fig. 12). In contrast, for positive tilting angles, the heater position plays a special role in determining the heat transfer performance of the cavity. In fact, for small values of D, i.e., $D < 0.3$ (see Fig. 8), the flow tends to separate from the discretely heated wall, at a point that moves slightly downwards with increasing the tilting angle of the cavity. Consequently, also the rising jet of warm fluid impinges upon the cooled sidewall at a point that shifts downwards with φ. This brings about a widening of the stagnation region located upstream the impingement point, thus implying that the amount of heat transferred to the upper portion of the cooled wall decreases with φ, as shown in Fig. 14, where the distributions of the local Nusselt number along the cooled wall are plotted for Ra = 10^5, $E = 0.2$, $D = 0.1$, and three different values of φ. The opposite behavior is instead observed for large values of D, i.e., $D > 0.5$ (see Fig. 9). In fact, in such case, the more the cavity is inclined, the more the breakdown of the fluid thermal stratification in the upper region of the enclosure is promoted, which leads to a significant increase of the heat transfer rate (see Fig. 12).

As regards the dependence of the optimum position of the heater on the cavity inclination, a set of distributions of Nu* vs. D are plotted in Fig. 15 for $E = 0.2$, Ra = 10^5, with φ as a parameter. It may be seen that D_{opt} either increases or decreases with the inclination of the enclosure according as the tilting angle is positive or negative. However, for negative angles the distribution of Nu* tends to be progressively smoother with increasing the inclination of the cavity, which implies that the amount of heat transferred across the enclosure tends to become practically independent of the heater location, and then the search for the value of D_{opt} loses almost completely of importance.

Finally, the effects of the Prandtl number are illustrated in Fig. 16, where the distributions of Nu* vs. Ra are plotted for $\varphi = 0°$, $D = 0.5$, $E = 0.2$, and different values of Pr. It may be noticed that the average Nusselt number increases with increasing the Prandtl

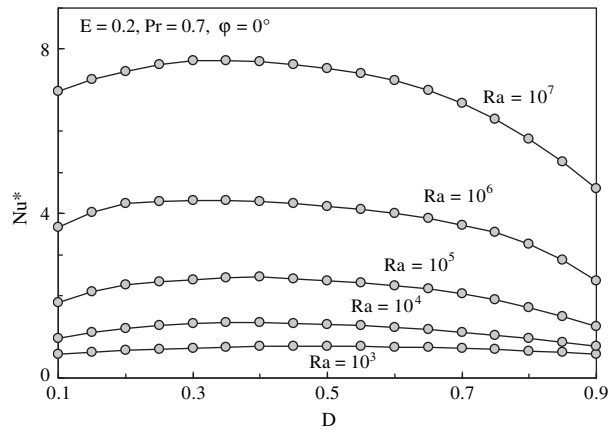

Fig. 11. Distributions of Nu* vs. D for Pr = 0.7, $\varphi = 0°$, $E = 0.2$ and Ra = 10^3–10^7.

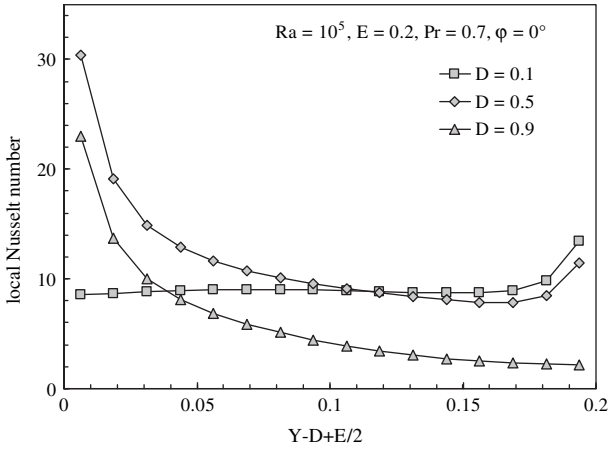

Fig. 13. Distributions of the local Nusselt number along the surface of the heater for Pr = 0.7, $\varphi = 0°$, Ra = 10^5, $E = 0.2$, and $D = 0.1 - 0.9$.

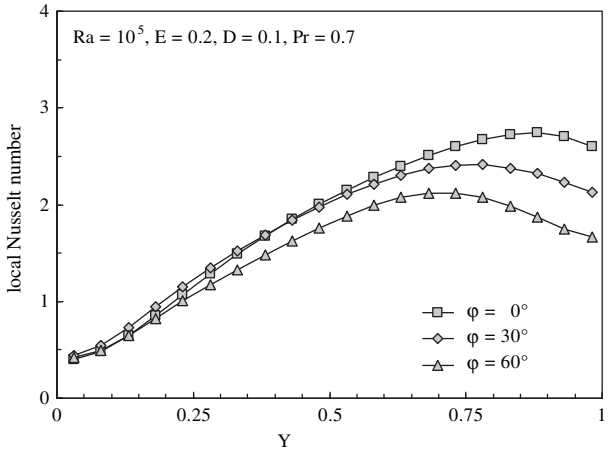

Fig. 14. Distributions of the local Nusselt number along the cooled wall for Pr = 0.7, Ra = 10^5, $E = 0.2$, $D = 0.1$ and $\varphi = 0^\circ$ to $+60^\circ$.

number, with a decreasing gradient, which is quite typical for intermediate Prandtl numbers. In addition, the distributions of the average Nusselt number for liquids maintain the same trends of those already derived for air, but the optimum location of the heater for maximum heat transfer tends to shift toward the bottom of the enclosure, i.e., D_{opt} tends to decrease, with increasing the Prandtl number, as e.g. reported in Fig. 17, where the distributions of Nu* vs. D are plotted for $\varphi = 0^\circ$, $E = 0.2$, Ra = 10^7, and different values of Pr.

The whole set of numerical results obtained for the optimum position D_{opt} of the heater for $10^3 \le Ra \le 10^7$, $0.7 \le Pr \le 700$, $\varphi \ge 0^\circ$ and $E \le 0.6$ (recall that the heater location ceases to be a meaningful independent variable for both negative inclinations of the cavity and too large sizes of the heater) may be correlated through the following algebraic equation, which is derived by a multiple regression procedure:

$$D_{opt} = 0.555\ Ra^{-0.0167}\left(\frac{E}{\cos\varphi^3\ Pr^{0.125}}\right)^{0.03\ln Ra-0.3} \tag{11}$$

with a 2.3% standard deviation of error and range of relative error between pairs of the raw data and the predictions from −9.7% to + 6.5%. Correspondingly, the Nusselt number Nu^*_{opt} of the discrete heat source located at the optimum position D_{opt} is given by the following algebraic equation:

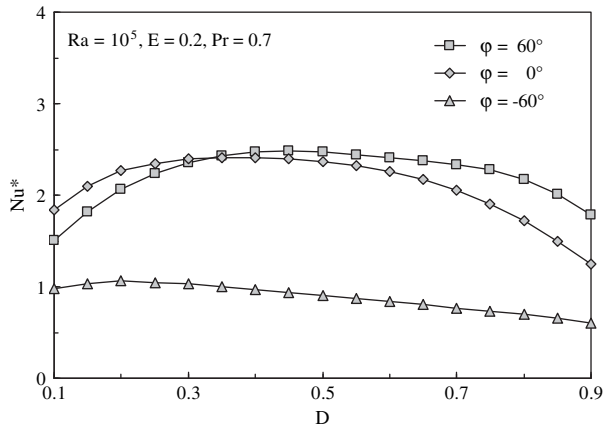

Fig. 15. Distributions of Nu* vs. D for Pr = 0.7, $E = 0.2$, Ra = 10^5 and $\varphi = -60^\circ$ to $+60^\circ$.

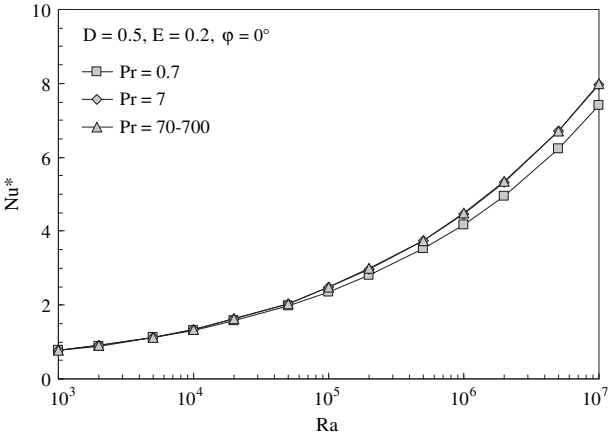

Fig. 16. Distributions of Nu* vs. Ra for $\varphi = 0^\circ$, $E = 0.2$, $D = 0.5$, and Pr = 0.7–700.

$$Nu^*_{opt} = \frac{1}{3.77}\left(\frac{Ra\ E^{1.5}Pr}{Pr + 0.2}\right)^{0.25} \tag{12}$$

with a 4.0% standard deviation of error and range of relative error from −6.4% to + 8.4%.

In addition, with specific reference to the vertical setting and to positive tilting angles of the cavity (i.e., $\varphi \ge 0^\circ$), which are undoubtedly the most attractive configurations by the thermal engineering design viewpoint, a multiple regression analysis of the numerical results obtained for the average Nusselt number Nu* of the heater for $0.1 \le E \le 1$, $E/2 \le D \le (1 - E/2)$, $10^3 \le Ra \le 10^7$, and $0.7 \le Pr \le 700$, produces the following semi-empirical correlating equations:

a) for $D \le D_{opt}$ and $E \le 0.6$

$$Nu^* = \frac{0.107}{A_\varphi + B_D}\left(\frac{Ra\ E^{1.5}\cos^3\varphi Pr}{Pr + 0.2}\right)^{0.25} \tag{13}$$

where

$$A_\varphi = 0.162 + 0.48\cos^3\varphi - 0.23\cos^6\varphi \tag{14}$$

$$B_D = (D_{opt} - D)^2 \tag{15}$$

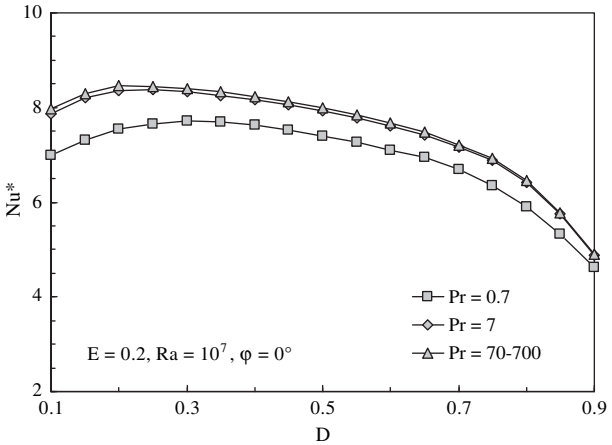

Fig. 17. Distributions of Nu* vs. D for $\varphi = 0^\circ$, $E = 0.2$, Ra = 10^7, and Pr = 0.7–700.

with a 5.8% standard deviation of error and a ±10% range of relative error with a 94% level of confidence;

b) for ($D > D_{opt}$ and $E \leq 0.6$) or ($E > 0.6$ and $\forall$D)

$$Nu^* = \frac{1}{3.6 + 39\ Ra^{-0.17} C_\varphi B_D} \left(\frac{Ra\ E^{1.5} Pr}{Pr + 0.2} \right)^{0.25} \quad (16)$$

where B_D is given by eq. (15) and

$$C_\varphi = 1 - 1.25\cos^3\varphi + 1.75\cos^6\varphi \quad (17)$$

with a 5.5% standard deviation of error and a ±10% range of relative error with a 95% level of confidence. Note that the value for D_{opt} to be employed in eq. (15) is the one obtained through eq. (11). In particular, this holds true also for $E > 0.6$, which implies the use of eq. (16), although eq. (11) is applicable only for $E \leq 0.6$, as indicated above. Therefore, it must be clear that the value of D_{opt} derived from eq. (11) for $E > 0.6$ has the only scope to calculate Nu^* through eq. (16), ceasing completely to have the meaning of optimum position of the heater for maximum heat removal.

5. Conclusions

Laminar natural convection heat transfer inside fluid-filled, tilted square cavities cooled at one side and partially heated at the opposite side, has been studied numerically. Simulations have been performed for different values of the ratio between the length of the heater and the width of the cavity, E, in the range between 0.1 and 1, the ratio between the distance of the center of the heater from the bottom endwall of the cavity and the width of the cavity, D, in the range between $E/2$ and $(1 - E/2)$, the Rayleigh number based on the width of the cavity, Ra, in the range between 10^3 and 10^7, the Prandtl number of the working fluid, Pr, in the range between 0.7 and 700, and the tilting angle of the enclosure with respect to the gravity vector, φ, in the range between $-75°$ and $+75°$.

New dimensionless correlating equations with substantially good standard deviations of error and ranges of error, have been developed for the average Nusselt number and the optimum heater location for maximum heat removal.

The main results obtained in the present study may be summarized as follows:

(a) The average Nusselt number increases with increasing the Rayleigh and Prandtl numbers, as well as with increasing the dimensionless size of the heater.
(b) For negative tilting angles, which correspond to configurations with the heater facing downwards, the amount of heat transferred across the enclosure degrades with increasing the cavity inclination.
(c) For positive inclinations, which correspond to configurations with the heater facing upwards, the heat transfer rate may either increase or decrease with increasing the tilting angle, according as the heater is located toward the top or the bottom of the enclosure.
(d) The average Nusselt number has a peak for intermediate positions of the discrete source, the higher are the Rayleigh and Prandtl numbers, the closer to the bottom of the cavity is such optimum location of the heater for maximum heat removal.
(e) For positive inclinations, the optimum heater location shifts toward the bottom of the enclosure with increasing the tilting angle, while the effect of the heater location on the thermal performance of the system is marginal for negative inclinations of the enclosure.

Nomenclature

D	dimensionless location of the heater
d	distance of the center of the heater from the bottom wall, m
E	dimensionless size of the heater
$\mathbf{g}$	gravity vector, m s^{-2}
g	gravitational acceleration, m s^{-2}
k	thermal conductivity of the fluid, W m^{-1} K^{-1}
L	length of the heater, m
Nu	average Nusselt number based on W
Nu*	average Nusselt number based on L
P	dimensionless pressure
Pr	Prandtl number
Q	dimensionless heat transfer rate per unit length
q	heat transfer rate per unit length, W m^{-1}
Ra	Rayleigh number based on W
T	dimensionless temperature
t	temperature, K
U	X-wise dimensionless velocity component
$\mathbf{V}$	dimensionless velocity vector
V	Y-wise dimensionless velocity component
W	width of the cavity, m
X,Y	dimensionless Cartesian coordinates

Greek symbols

α	thermal diffusivity of the fluid, m^2 s^{-1}
β	coefficient of volumetric thermal expansion of the fluid, K^{-1}
ν	kinematic viscosity of the fluid, m^2 s^{-1}
ρ	density of the fluid, kg m^{-3}
τ	dimensionless time
φ	tilting angle of the enclosure with respect to gravity, deg
ψ	dimensionless stream function

Subscripts

C	cold
H	hot
in	incoming
max	maximum value
opt	optimum
out	outgoing

References

[1] H.H.S. Chu, S.W. Churchill, C.V.S. Patterson, The effect of heater size, location, aspect ratio, and boundary conditions on two-dimensional, laminar, natural convection in rectangular channels. J. Heat Transfer 98 (1976) 194–201.
[2] B.L. Turner, R.D. Flack, The experimental measurement of natural convective heat transfer in rectangular enclosure with concentrated heat sources. J. Heat Transfer 102 (1980) 236–241.
[3] M. Keyhani, V. Prasad, R. Cox, An experimental study of natural convection in a vertical cavità with discrete heat sources. J. Heat Transfer 110 (1988) 616–624.
[4] M.L. Chadwick, B.W. Webb, H.S. Heaton, Natural convection from two-dimensional discrete heat sources in a rectangular enclosure. Int. J. Heat Mass Transfer 34 (1991) 1679–1693.
[5] G. Refai Ahmed, M.M. Yovanovich, Influence of discrete heat source location on natural convection heat transfer in a vertical square enclosure. J. Electronic Packaging 113 (1991) 268–274.
[6] G. Refai Ahmed, M.M. Yovanovich, Numerical study of natural convection from discrete heat sources in a vertical square enclosure. J. Thermophysics 6 (1992) 121–127.
[7] C.J. Ho, J.Y. Chang, A study of natural convection heat transfer in a vertical rectangular enclosure with two-dimensional discrete heating: effect of aspect ratio. Int. J. Heat Mass Transfer 37 (1994) 917–925.

[8] M.S. Polentini, S. Ramadhyani, F.P. Incropera, Single-phase thermosyphon cooling of an array of discrete heat sources in a rectangular cavità. Int. J. Heat Mass Transfer 36 (1993) 3983–3996.
[9] T.J. Heindel, S. Ramadhyani, F.P. Incropera, Laminar natural convection in a discretely heated cavity: I–assessment of three-dimensional effects. J. Heat Transfer 117 (1995) 902–909.
[10] T.J. Heindel, S. Ramadhyani, F.P. Incropera, Laminar natural convection in a discretely heated cavity: II–comparisons of experimental and theoretical results. J. Heat Transfer 117 (1995) 910–917.
[11] S.K.W. Tou, C.P. Tso, X. Zhang, 3-D numerical analysis of natural convective liquid cooling of a 3 × 3 heater array in rectangular enclosures. Int. J. Heat Mass Transfer 42 (1999) 3231–3244.
[12] S.K.W. Tou, X.F. Zhang, Three-dimensional numerical simulation of natural convection in an inclined liquid-filled enclosure with an array of discrete heaters. Int. J. Heat Mass Transfer 46 (2003) 127–138.
[13] C.P. Tso, L.F. Lin, S.K.W. Tou, X. Zhang, Flow pattern evolution in natural convection from an array of discrete heat sources in a rectangular cavity at various orientations. Int. J. Heat Mass Transfer 47 (2004) 4061–4073.
[14] Y. Liu, N. Phan-Tien, An optimum spacing problem for three chips mounted on a vertical substrate in an enclosure. Num. Heat Transfer 37 (2000) 613–630.
[15] A.K. da Silva, S. Lorente, A. Bejan, Optimal distribution of discrete heat sources on a wall with natural convection. Int. J. Heat Mass Transfer 47 (2004) 203–214.
[16] A.K. da Silva, S. Lorente, A. Bejan, Constructal multi-scale structures for maximal heat transfer density. Energy 31 (2006) 620–635.
[17] R.L. Frederick, F. Quiroz, On the transition from conduction to convection regime in a cubical enclosure with a partially heated wall. Int. J. Heat Mass Transfer 44 (2001) 1699–1709.
[18] Y.L. He, W.W. Yang, W.Q. Tao, Three-dimensional numerical study of natural convective heat transfer of liquid in a cubic enclosure. Num. Heat Transfer 47 (2005) 917–934.
[19] A. Baïri, J.M. García de María, N. Laraqi, N. Alilat, Free convection generated in an enclosure by alternate heated bands. Experimental and numerical study adapted to electronics thermal control. Int. J. Heat Fluid Flow 29 (2008) 1337–1346.
[20] N. Nithyadevi, P. Kandaswamy, J. Lee, Natural convection in a rectangular cavity with partially active side walls. Int. J. Heat Mass Transfer 50 (2007) 4688–4697.
[21] Q.-H. Deng, Fluid flow and heat transfer characteristics of natural convection in square cavities due to discrete source-sink pairs. Int. J. Heat Mass Transfer 51 (2008) 5949–5957.
[22] K.T. Yang, Transitions and bifurcations in laminar buoyant flows in confined enclosures. J. Heat Transfer 110 (1988) 1191–1204.
[23] M. Cappelli D'Orazio, C. Cianfrini, M. Corcione, Rayleigh-Bénard convection in tall rectangular enclosures. Int. J. Thermal Sci. 43 (2004) 135–144.
[24] J.P. Van Doormaal, G.D. Raithby, Enhancements of the simple method for predicting incompressible fluid flows. Num. Heat Transfer 11 (1984) 147–163.
[25] S.V. Patankar, D.B. Spalding, A calculation procedure for heat, mass and momentum transfer in three-dimensional parabolic flows. Int. J. Heat Mass Transfer 15 (1972) 1787–1797.
[26] B.P. Leonard, A stable and accurate convective modelling procedure based on quadratic upstream interpolation. Comp. Meth. Appl. Mech. Engng. 19 (1979) 59–78.
[27] S.V. Patankar, Numerical Heat Transfer and Fluid Flow. Hemisphere Publ. Co., Washington, DC, 1980.
[28] G. de Vahl Davis, Natural convection of air in a square cavity: a bench mark numerical solution. Int. J. Num. Meth. Fluids 3 (1983) 249–264.
[29] H.S. Mahdi, R.B. Kinney, Time-dependent natural convection in a square cavity: application of a new finite volume method. Int. J. Num. Meth. Fluids 11 (1990) 57–86.
[30] M. Hortmann, M. Peric, G. Scheuerer, Finite volume multigrid prediction of laminar natural convection: bench-mark solutions. Int. J. Num. Meth. Fluids 11 (1990) 189–207.
[31] D.C. Wan, B.S.V. Patnaik, G.W. Wei, A new benchmark quality solution for the buoyancy-driven cavity by discrete singular convolution. Num. Heat Transfer 40 (2001) 199–228.
[32] A. Bejan, Convection Heat Transfer, third ed. John Wiley & Sons, Inc., Hoboken, New Jersey, 2004.
[33] F.P. Incropera, D.P. Dewitt, T.L. Bergman, A.S. Lavine, Fundamentals of Heat and Mass Transfer, sixth ed. John Wiley & Sons, Inc., Hoboken, New Jersey, 2007.